

S.P. Sridhar¹, S. Arun Kumar², P. Sathiya^{1*}¹*Department of Production Engineering, National Institute of Technology, Tiruchirappalli-620015, Tamilnadu, India*²*School of mechanical engineering, SASTRA University, Thanjavur-613401, Tamilnadu, India** *psathiya@nitt.edu*

A STUDY ON THE EFFECT OF DIFFERENT ACTIVATING FLUX ON A-TIG WELDING PROCESS OF INCOLOY 800H

ABSTRACT

This study investigates the effect of different activating flux such as V_2O_5 , TiO_2 , MoO_3 , Cr_2O_3 , and Al_2O_3 on A-TIG welding process of Incoloy 800H. The influence of the flux on the depth of penetration and on mechanical and metallurgical characteristics of the weld were studied and compared with autogeneous TIG welds which were welded with the same process parameters and conditions. The use of TiO_2 flux gave full depth of penetration and the use of V_2O_5 , Cr_2O_3 flux gave increased penetration as compared to autogeneous TIG welds while the use of Al_2O_3 and MoO_3 led to the deterioration of the effect.

Key words: A-TIG, Incoloy 800H, Activating Flux, Carbide, Corrosion

INTRODUCTION

Incoloy 800H (UNS N08810), which comes under the group of austenitic nickel-iron chromium steel, exhibits resistance to the carburization, corrosion and oxidation at high temperature. The combination of appreciable strength and corrosion resistance in a series of elevated temperature makes this alloy useful in many applications such as cracker tubes in petrochemical furnace, headers and pigtailed, fourth generation nuclear power plant components, equipment and furnace components etc. [1]. GTAW process is preferred for producing high quality weld joint where control of weld bead and shape is possible ensuring the metallurgical stability of the welded joints. On the other hand the major disadvantages of TIG welding process are the low productivity due to the number of passes required when welding thick sections and the requirement of highly skilled welders. To overcome these disadvantages, A-TIG welding process, a variant of TIG welding process, was developed by Paton Electric Welding Institute (1960). In this process a thin layer of fluxes (oxide, halide, fluoride and chloride) was applied on the region where the weld was to be made. The activating flux improved the depth of penetration up to 300% as compared to autogeneous TIG welding [2]. The reversed Marangoni convection and the arc constriction effect were considered as the two major mechanisms for the increased depth of penetration in A-TIG welding process [3]. But research is still going on to find the exact mechanism which causes

the depth of penetration. A-TIG welding process was carried out in Nimonic 263 alloy with three fluxes and the results suggested that as the thickness of the flux coating increased, the depth of penetration decreased. The fluxes did not decompose fully and this affected the viscosity of the molten metal flow and hence resulted in lower depth of penetration [4]. A-TIG welding was done on stainless steel (0Cr18Ni9) with two different activating fluxes SiO_2 and TiO_2 . The increased depth of penetration using SiO_2 flux was due to arc constriction effect and reversed Marangoni convection whereas the increase in depth of penetration by using TiO_2 flux was only due to reversed Marangoni convection [5]. Sakthivel et al. compared the creep strength of TIG & A-TIG welded austenitic 316LN steel and concluded that the A-TIG weldments had lower creep rupture life than the TIG weldments because the TIG welded joints had lower weld strength reduction factor as compared to the A-TIG joints [6]. Devendranath Ramkumar et al. performed A-TIG welding on 904L super austenitic stainless steel with the use of 85% SiO_2 + 15% TiO_2 and reported that the weld penetration increased three times as compared to the autogeneous TIG weld. A-TIG weldments failed in the weld zone in tensile testing due to the lower hardness in the weld region as compared to the base material and HAZ [7]. Monoj Kumar et al. investigated the tensile properties of A-TIG in Inconel 718 joints welded using SiO_2 & TiO_2 flux. The TiO_2 A-TIG weldments had higher tensile strength as compared to SiO_2 weldments and also the A-TIG joints had higher strength than that of the parent material [8]. Shyu et al. reported that the increased δ ferrite content in the weld zone of A-TIG welded austenitic stainless steel improved the mechanical properties such as ductility, hardness and strength than the TIG welded joints [9]. The combination of 50% SiO_2 + 50% MoO_3 and SiO_2 flux reduced the hot cracking susceptibility on Inconel 718 weldments and the higher depth to width ratio was obtained using 50% SiO_2 + 50% MoO_3 and 50% SiO_2 + 50% NiO flux combination [10]. Sairam et al. performed dissimilar welding of Incoloy 800H and austenitic stainless steel (321) by using two different filler material, Inconel 617 and Inconel 82 [11]. In this work an attempt is made to find the effect of different activating flux on A-TIG welding process of Incoloy 800H. The depth of penetration, mechanical and metallurgical characteristics of the weldments were analysed.

EXPERIMENTAL PROCEDURE

Incoloy 800H of dimension 100x75x4 mm was chosen as the base material. The chemical composition of Incoloy 800H is shown in Table 1. Five different fluxes (TiO_2 , Cr_2O_3 , MoO_3 , V_2O_5 , and Al_2O_3) were mixed with acetone in the ratio of 1:6.5 separately to form a paste. A thin layer of flux coating was applied on the region where the weld was to be made. Prior to the application of flux, the base material was cleaned with emery sheets and acetone to keep the surface away from contaminants. A-TIG welding and autogeneous TIG welding were performed using Lincoln TIG welding machine and the process parameters used to complete the weld are shown in Table 2. After welding the weldments were cut in the cross section of the weldments using a wire cut EDM machine to analyse the effect of different flux on the mechanical and metallurgical characteristics of the weldments. The schematic representation of coupons obtained from the A-TIG weldments for mechanical and metallurgical characterization is shown in fig. 1. The cross sectioned weldments were polished with different grade of emery sheets followed by alumina and diamond polishing to get mirror finish. The etchant with the combination of 15 ml HCL + 10 ml HNO_3 + 10 ml CH_3COOH was used to reveal the macro and microstructure of the welded joints. The depth and width of

the weld bead were measured using IMAGE-J software. The SEM with EDS analysis was made using Carl Zeiss σ version machine in high vacuum mode. The hardness was measured using Vickers micro hardness tester, loaded with 500 g for a dwell time of 15 s transverse cross-section of the weldments at different locations.

Table 1. Chemical elements of Incoloy 800H

C	Mn	S	Si	Cu	Cr	Fe	Al	Ti	Ni
0.065	0.688	<0.010	0.094	0.091	20.79	46.60	0.277	0.280	30.65

Table 2. Welding parameters

Parameters	Values	Units
Welding Current	100	Amps
Arc Length	2	mm
Shielding Gas	Argon	99.999% pure
shielding gas flow rate	15	lpm
		\emptyset
Electrode Diameter	2.4	
Welding Speed	50	mm/min
Power Polarity	DCEN	
Electrode type	2%-wt ThO ₂ thoriated tungsten.	

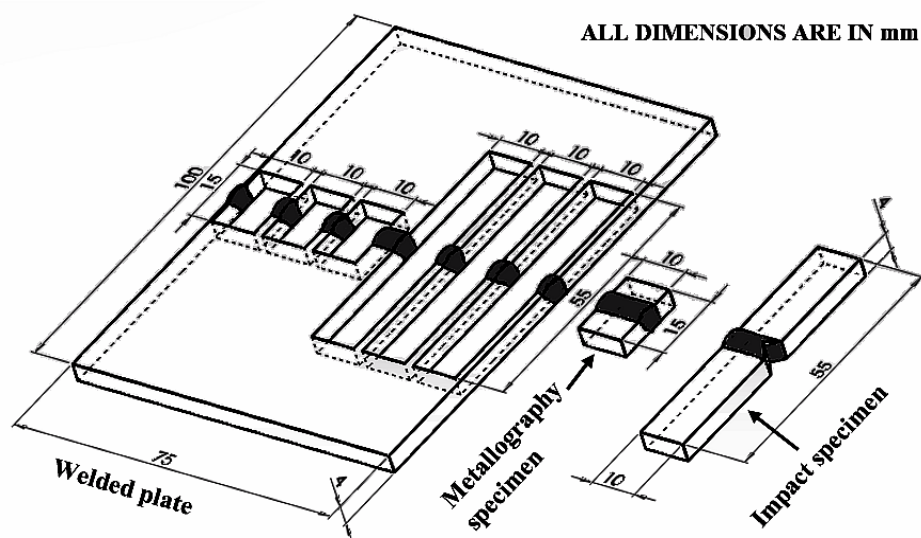


Fig. 1. Schematic representation of coupons obtained from the A-TIG weldments for metallurgical and mechanical characterization studies

RESULT AND DISCUSSION

Macrostructure of the weld region

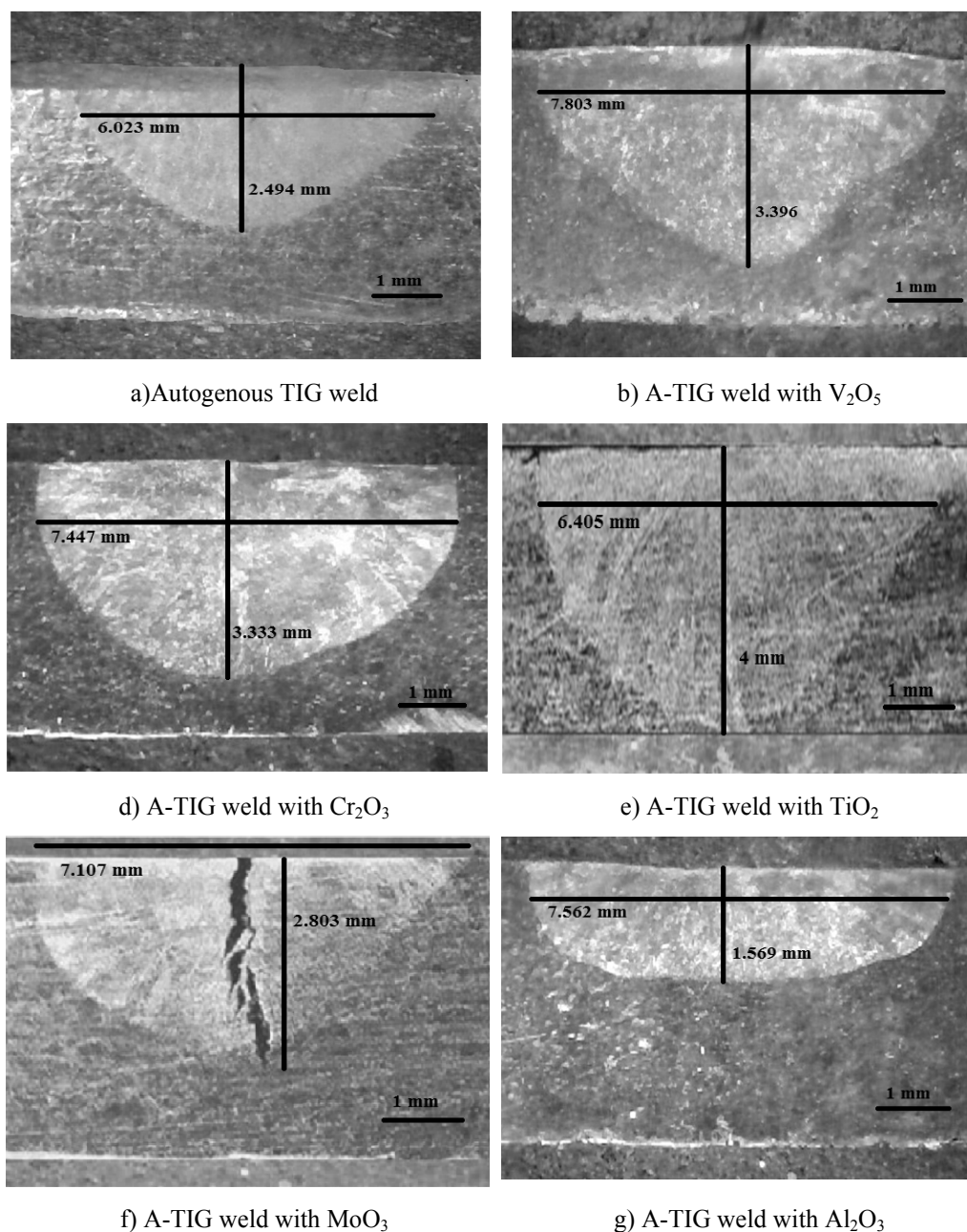


Fig. 2. Macrostructure of the weldments

Fig. 2 shows the macrostructure of the autogeneous TIG and A-TIG weldments. From the figure 2 (a) it can be seen that the autogeneous TIG gave a weld depth of 2.494 mm. Compared to the autogeneous weld zone depth, the use of TiO_2 flux (fig. 2 (e)) gave a full

depth penetration and V_2O_5 , Cr_2O_3 flux (fig. 2 (b & d)) gave a deeper penetration. The use of Al_2O_3 flux (fig. 2 (g)) gave a lesser depth of penetration. Most likely the increased depth in penetration was due to the reversed Marangoni convection which relates the penetration depth to the fluid flow direction. The molten fluid flow direction is determined by the temperature co-efficient of surface tension. In TIG welding the convection movements were centrifugal and surface tension gradient in negative led to shallow penetration. The addition of activating flux improved the oxygen content which induced an inversion of the convection currents changing the sign of the surface tension gradient from negative to positive and the resulting convection current movements changed to centripetal. Hence the depth of penetration increased [12]. Also the depth of penetration depended upon the interaction between base material composition and the flux, the type of flux used and the process parameters involved during the welding [9]. The use of MoO_3 flux led to hot cracking issue in Incoloy 800H whereas this defect was not reported in materials such as duplex stainless steel, Inconel 718 and 316L austenitic stainless steel [13-16]. Hot cracking is a welding defect that occurs with

temperature higher than 1200^0 C and it is due to the presence of impurities with lower melting

than the base metal. The cooling is greater on the weld region and it is from there that grain grows forwards the centre of the weld which is the last to become solid. Since almost all alloys, solidify over a range of temperature, the first metal to solidify will have higher melting point and the last will have the lowest melting point. As a consequence of this, the lowest melting point composition is pushed ahead of the solidifying dendrite until it gets trapped between the adjacent dendrites, along the grain boundaries. If the difference in melting point between the lowest melting point constraint and rest of the bulk material is sufficiently great, the liquid films by the grain boundaries will be separated as cools and contracts leading to hot cracking. Some theories suggest that hot cracking is dependent on the metallurgical and mechanical factors that are supposed to be independent of each other [17-18]. Further studies have also shown that cracking could also be initiated at the early stage of solidification [19].

Microstructure of the base material

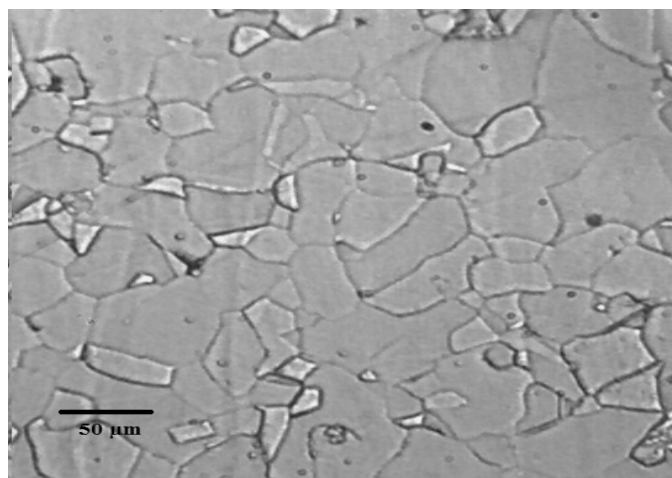


Fig. 3. Microstructure of the base material

Fig. 3 shows the microstructure of the base material Incoloy 800H as received in mill and annealed condition which was solution treated at a temperature of approximately 1150°C to promote grain growth and dissolution of carbides. This left some of the carbon available for precipitation during service. The microstructure consisted of a solid solution matrix in which some grains were delineated by intergranular carbonitrides and by twinning lines.

Microstructure of the weld region

Fig. 4 shows the microstructure of the weld of autogeneous TIG weld and A-TIG welds with the use of different activating fluxes.

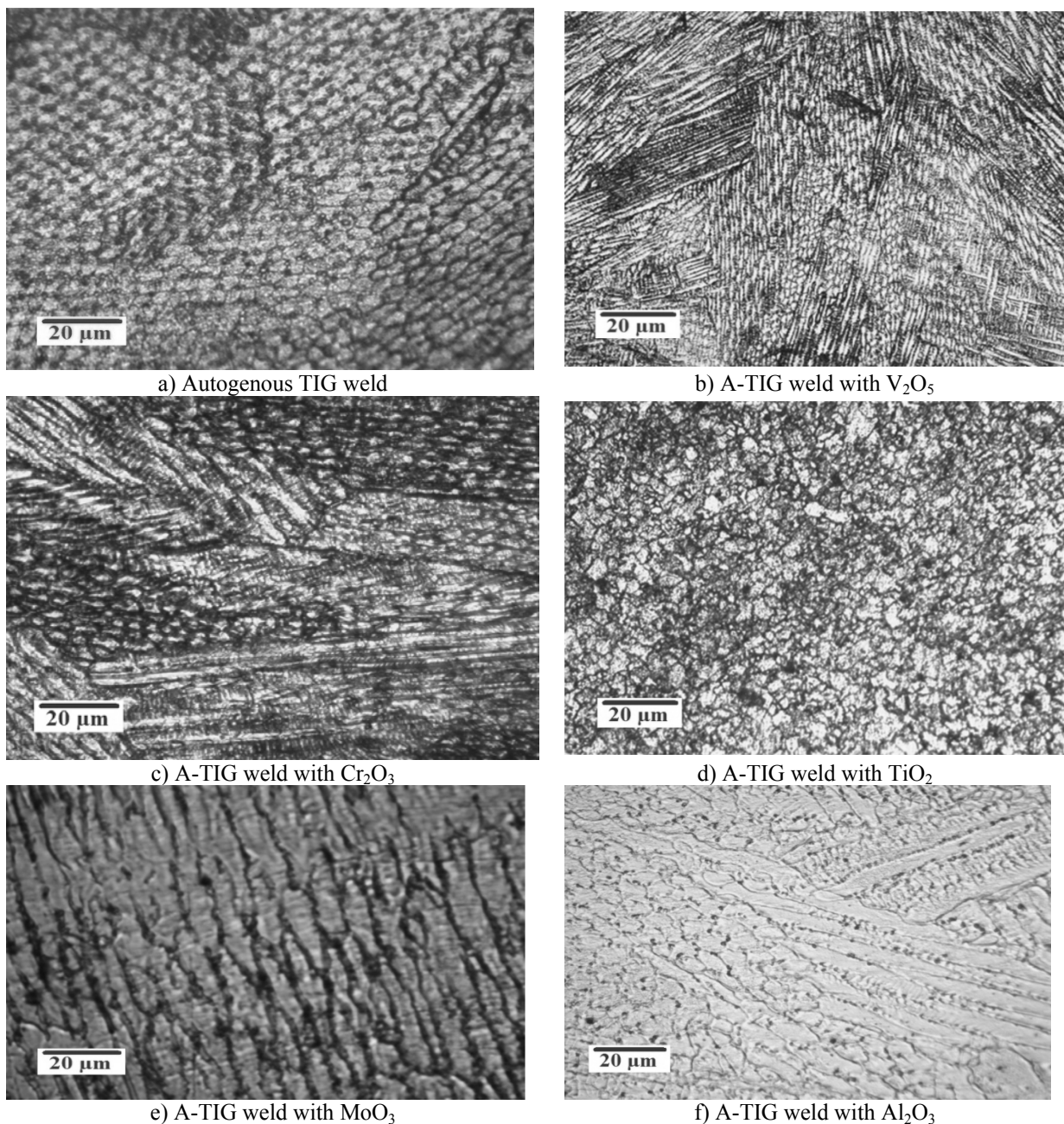


Fig. 4. Microstructure of the autogeneous TIG weld and A-TIG

It can be seen from the figures that each flux gave different microstructure in the weld region. The autogeneous weld region exhibited equiaxed grain structure and TiO_2 flux gave a much finer grain equiaxed grain structure as compared with the autogeneous welds. The equiaxed grain structure is most preferred structure because it can exhibit higher strength than the other solidification structures. The use of Cr_2O_3 and V_2O_5 flux produced a combination of equiaxed and columnar structure throughout the weld region but the V_2O_5 flux exhibited much finer grains. The advantage of combination that fine grain sizes confer on metal structures is unique; as it increases strength, toughness and fatigue life [20-21]. The Al_2O_3 and MoO_3 flux led to the formation of coarser dendritic structures which was not preferred in most welding application, as dendrites were more prone to cracking. It is also seen that the use of MoO_3 flux caused solidification cracking in the weld metal. There are certain stages, there are certain particular patterns or the modes through which solidification takes place and these modes basically, dictate the structure of the weld, which is developed after the solidification. And these modes of the solidification depend upon the composition of the weld metal and the cooling conditions experienced during the welding, and this means that, the solidification can take place in different modes like planar, cellular, dendritic and the equiaxed. The actual temperature gradient (G) and growth rate (R) have a major influence on the solidification mode. A combination of high G and low R results in planar solidification, A combination of low G and high R results in equiaxed solidification and the combination of intermediate values of G and R results in the cellular and dendrite mode of solidification [22].

XRD analysis of the weld region

Fig. 5 Presents the XRD results of the weld region, welded with the application of different flux.

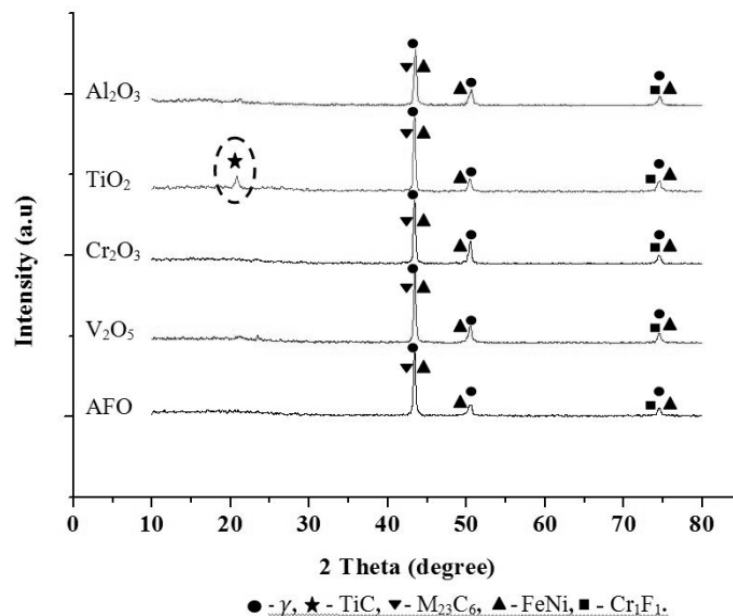


Fig. 5. XRD results of the weld region

The XRD peaks were searched using X'Pert High Score Plus software to find the possible phase transformation during welding. The phase identified was the austenite phase (γ) as nickel is a stabilizer. Iron nickel carbides ($M_{23}C_6$) and chromium nickel carbides were formed for all the weldments. The $M_{23}C_6$ carbides form near the grain boundaries. When the grain boundary is much finer, the $M_{23}C_6$ will be beneficial to the fatigue property of the alloy, strengthening the grain boundary and preventing the migration of grain boundaries during deformation [23]. The weld using TiO_2 flux alone showed the formation titanium carbides (TiC). These carbides do not dissolve in elevated temperature environment and the grain boundaries can thus enhance the fracture resistance of the material [24].

Fractography analysis

The Fig. 6 shows the impact tested specimen of the TiO_2 welds which gave full depth of penetration.

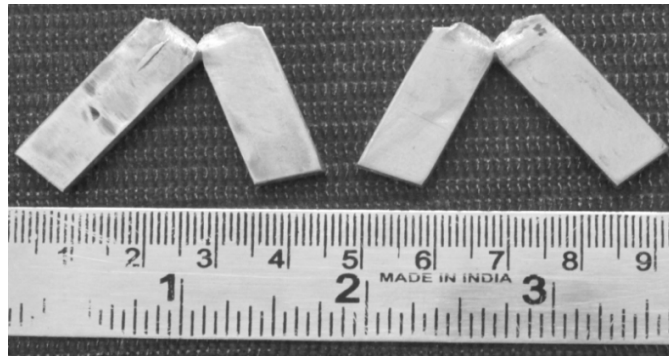


Fig. 6. Photograph of the Impact tested specimen

Two samples were prepared and tested by making a V-notch at the centre of the weld. The toughness obtained was 72 J and 75J respectively and it was higher than the TIG welded joints (60 J) as reported by Arun Kumar et al. [25]. Further the fractured surface was analysed through SEM at two different locations and is shown in Fig. 7. The figure clearly depicts mostly voids and dimples which corresponded to the ductile mode of fracture.

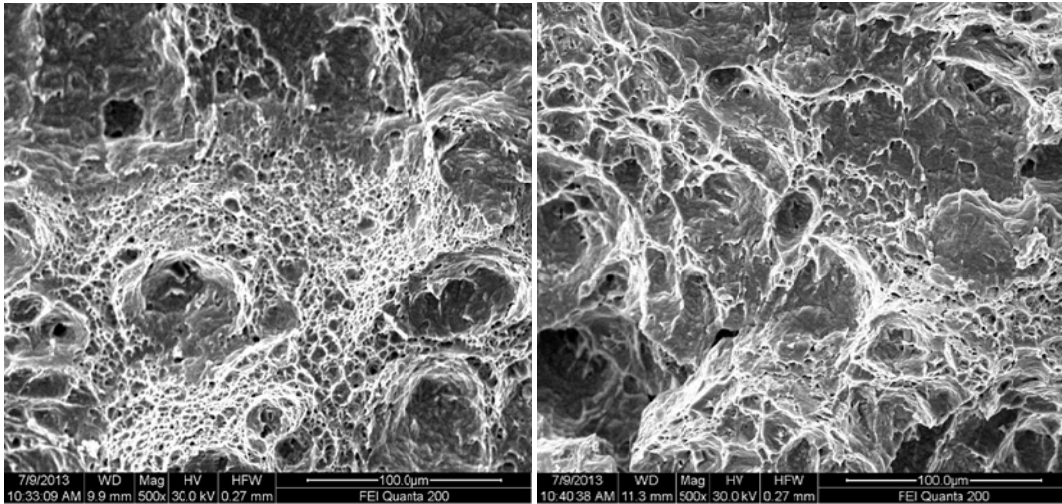


Fig. 7. Fractography of the impact tested specimen

Hardness

The fig.8 shows the hardness profile of the welds.

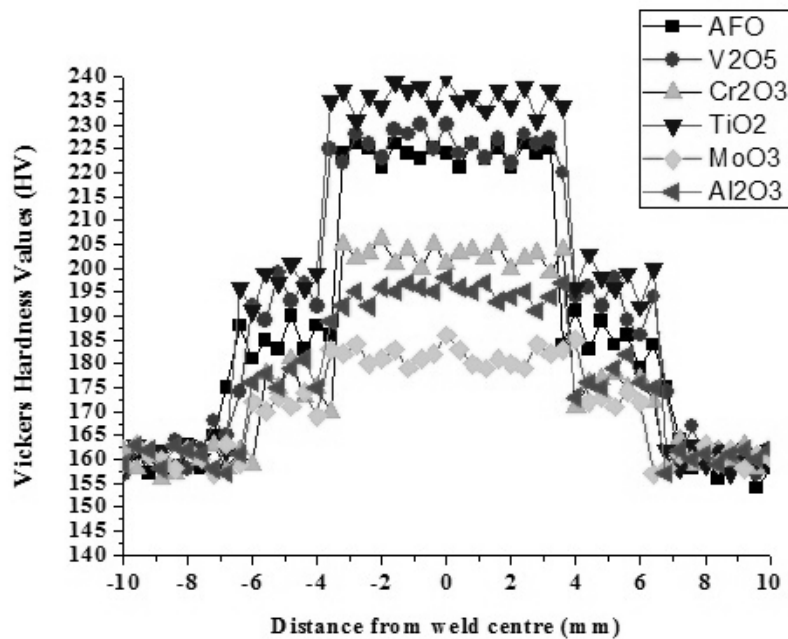


Fig. 8. Hardness profile of the welds

The TiO_2 weld and V_2O_5 welds exhibited higher hardness (240 & 230 HV) than the autogenous welds (226 HV). This may be due to fine grain size and formation of the titanium carbides in the weld region of the TiO_2 welds. The low hardness of the other welds as compared to the autogenous weld may be due to coarser grain structure obtained in the weld region.

Corrosion Analysis

The potentiodynamic polarization test was carried for the base material and TiO₂ weldments. Two tests were carried out for the weld region to check the repeatability of the results. 1 mole of NaCl mixed in one litre of distilled water was used as the electrolytic solution. 1 hour of stabilizing time was given before each polarisation scan. The local polarization curve was plotted from -1 V to 1 V at a scan rate of 0.5 mV/s. The fig. 9 shows the polarization curves taken for the base material and two weldments. From the Figure it can be seen that the current density was less for the weldments which means that the loss of electrons was less thus providing better corrosion resistance compared to the base material. This may be due to the fine grain size, the formation of iron chromium carbides and titanium carbides in the weld region. Also both the weld samples exhibited similar polarization curves.

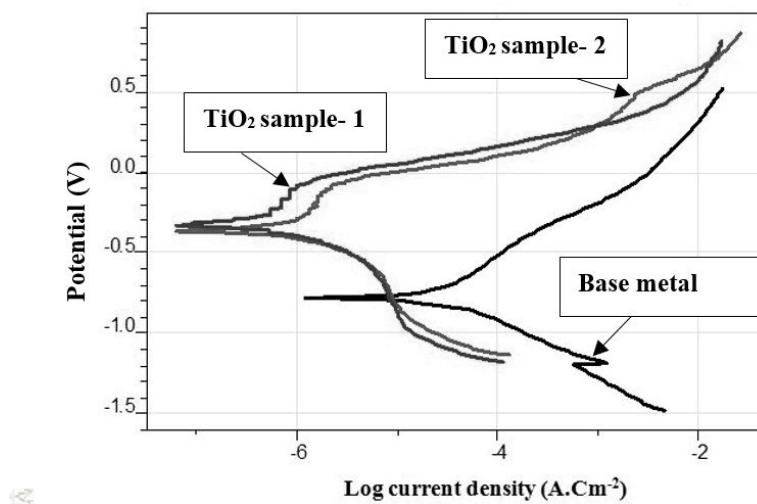


Fig. 9. Tafel plot

CONCLUSIONS

The A-TIG welding was carried on Incoloy 800H with different flux (V₂O₅, TiO₂, Cr₂O₃, MoO₃ and Al₂O₃). Full depth of penetration was observed in A-TIG welding process for 4 mm thick Incoloy 800H plates by using TiO₂ as an activating flux. An increase in penetration of 133% was obtained for V₂O₅ and Cr₂O₃ flux as compared to the autogeneous TIG weld. The reversed Marangoni convection was the cause for the increased depth of penetration. The use of MoO₃ caused solidification cracking in the weldment. The use of TiO₂ and V₂O₅ flux showed finer grain size and higher hardness in the weld region as compared to other welds. The XRD peaks revealed the formation of titanium carbides in the weld region of TiO₂ welds which would give resistance to fracture. The toughness of TiO₂ weldments was more when compared to the TIG welded Incoloy 800HT joints. The TiO₂ weldments had improved corrosion resistance as compared to the autogeneous TIG welded joints.

REFERENCES

1. <http://www.specialmetals.com/assets/documents/alloys/incoloy/incoloy-alloy-800.pdf>
2. Paulo J. Modenesi., Eustaquo R. Apolinario., Iaci M. Pereira., TIG welding with single-component fluxes. *Journal of Materials Processing Technology*, 99 (2000), 260-265.
3. Kuang-Hung Tseng, Chih-Yu Hsu. Performance of activated TIG process in austenitic stainless steel welds. *Journal of Materials Processing Technology*, 211 (2011), 503–512.
4. Xu Y.L., Dong Z.B., Wei Y.H., Yang C.L., Marangoni convection and weld shape variation in A-TIG welding process. *Theoretical and Applied Fracture Mechanics*, 48 (2007), 178–186.
5. Chunli YANG., Sanbao LIN., Fengyao LIU., Lin WU., Qingtao ZHANG., Research on the Mechanism of Penetration Increase by Flux in A-TIG Welding. *Journal of Materials Science & Technology*, 19(1) (2003), 225-227.
6. Sakthivel T., Vasudevan M., Laha K., Parameswaran P., Chandravathi K.S., Mathew M.D., Bhaduri A.K., Comparison of creep rupture behaviour of type 316L(N) austenitic stainless steel joints welded by TIG and activated TIG welding processes. *Materials Science and Engineering: A*, 528 (2011), 6971– 6980.
7. Devendranath Ramkumar K., Jelli Lakshmi Narasimha Varma., Gangineni Chaitanya., Ayush Choudhary., Arivazhagan N., Narayanan S., Effect of autogeneous GTA welding with and without flux addition on the microstructure and mechanical properties of AISI 904 L joints. *Materials Science and Engineering: A*, 636 (2015), 1-9.
8. Devendranath Ramkumar K., Monoj Kumar B., Gokul Krishnan M., Sidarth Dev., Aman Jayesh Bhalodi., Arivazhagan N., Narayanan S., Studies on the weldability, microstructure and mechanical properties of activated flux TIG weldments of Inconel 718. *Materials Science and Engineering: A*, 639 (2015), 234–244.
9. Shyu S.W., Huang HY., Tseng K H., Chou C.P., Study of the Performance of Stainless Steel A-TIG Welds. *Journal of Materials Engineering and Performance*, 17 (2008), 193–201.
10. Hsuan-Liang Lin., Tong-Min Wu., Ching-Min Cheng., Effects of Flux Precoating and Process Parameter on Welding Performance of Inconel 718 Alloy TIG Welds. *Journal of Materials Engineering and Performance*, 23 (2014), 125–132.
11. Sayiram G., Arivazhagan N., Microstructural characterization of dissimilar welds between Incoloy 800H and 321 Austenitic Stainless Steel. *Materials Characterization*, 102 (2015), 180–188.
12. Rui-Hua ZHANG., Ji-Luan PAN., Seiji KATAYAMA., The mechanism of penetration increase in A-TIG welding. *Frontiers of Materials Science*, 5(2) (2011), 109–118.
13. Tsann-Shyi Chern., Kuang-Hung Tseng., Hsien-Lung Tsai., Study of the characteristics of duplex stainless steel activated tungsten inert gas welds. *Materials and Design*, 32 (2011), 255–263.
14. Kuang-Hung Tseng., Chih-Yu Hsu., Performance of activated TIG process in austenitic stainless steel welds. *Journal of Materials Processing Technology*, 211 (2011), 503–512.
15. Hsuan-Liang Lin., Tong-Min Wu., Effects of Activating Flux on Weld Bead Geometry of Inconel 718 Alloy TIG Welds. *Materials and Manufacturing Processes*, 27 (2012), 1457–1461.
16. Kuang-Hung Tseng., Development and application of oxide-based flux powder for tungsten inert gas welding of austenitic stainless steels. *Powder Technology*, 233 (2013), 72–79.
17. Fink C., Keil D., Zinke M., Evaluation of hot cracking susceptibility of nickel-based alloys by the pvr test. *Welding in the World*, 56(7) (2012), 37-43.

18. Borland J C., Younger R N., Some aspects of cracking in welded Cr–Ni austenitic steels. *British Welding Journal*, 7 (1960), 22–59.
19. Matsuda F., Nakagawa H., Sorada K., Dynamic observation of solidification and solidification cracking during welding with optical microscope. *Transactions of the Japan Welding Research Institute*, 11 (1982), 67–77.
20. Hall EO., The Deformation and Aging of Mild steel. *Proceedings of the Physical Society*, 64B (1951), 747-753.
21. Garstone J., Johnson FA., Impact Properties of Mild Steel Weld Metals. *British Welding Journal*, 10(5) (1963), 224.
22. Sindo Kou.: *Welding Metallurgy*. Second Edition. John Wiley & Sons, Incorporated, Hoboken, NJ, USA, 2003.
23. He L Z., Zheng Q., Sun X F., Hou GC., Guan H R., Hu ZQ., M23C6 precipitation behavior in a Ni-base superalloy M963. *Journal of Materials Science*, 40 (11) (2005), 2959-2964.
24. Sireesha M., Shankar V., Shaju K Albert., Sundaresan S., Microstructural features of dissimilar welds between 316LN austenitic stainless steel and alloy 800. *Materials Science and Engineering: A*, 292 (1) (2000), 74-82.
25. Arun Kumar Srirangan., Sathiya Paulraj., Multi-response optimization of process parameters for TIG welding of Incoloy 800HT by Taguchi grey relational analysis. *Engineering Science and Technology, an International Journal*. doi:10.1016/j.jestch.2015.10.003.